THE JOURNAL OF BIOLOGICAL CHEMISTRY VOL. 284, NO. 34, pp. 22664–22671, August 21, 2009

ADP-dependent 6-Phosphofructokinase from *Pyrococcus horikoshii* OT3

STRUCTURE DETERMINATION AND BIOCHEMICAL CHARACTERIZATION OF PH1645[*][S]

Received for publication, April 24, 2009, and in revised form, June 22, 2009 Published, JBC Papers in Press, June 24, 2009, DOI 10.1074/jbc.M109.012401

Mark A. Currie[‡1], **Felipe Merino**[§1], **Tatiana Skarina**[¶1], **Andrew H. Y. Wong**[‡], **Alexander Singer**[¶], **Greg Brown**[¶], **Alexei Savchenko**[¶], **Andrés Caniuguir**[§], **Victoria Guixé**[§], **Alexander F. Yakunin**[¶], **and Zongchao Jia**[‡2]

From the [‡]*Department of Biochemistry, Queen's University, Kingston, Ontario K7L 3N6, Canada, the* [§]*Departamento de Biología, Facultad de Ciencias, Universidad de Chile, Casilla 653, Santiago, Chile, and the* [¶]*Midwest Center for Structural Genomics, Toronto, Ontario M5G 1L6, Canada*

Some hyperthermophilic archaea use a modified glycolytic pathway that employs an ADP-dependent glucokinase (ADP-GK) and an ADP-dependent phosphofructokinase (ADP-PFK) or, in the case of *Methanococcus jannaschii*, a bifunctional ADP-dependent glucophosphofructokinase (ADP-GK/PFK). The crystal structures of three ADP-GKs have been determined. However, there is no structural information available for ADP-PFKs or the ADP-GK/PFK. Here, we present the first crystal structure of an ADP-PFK from *Pyrococcus horikoshii OT3* (*Ph*PFK) in both apo- and AMP-bound forms determined to 2.0-Å and 1.9-Å resolution, respectively, along with biochemical characterization of the enzyme. The overall structure of *Ph*PFK maintains a similar large and small α/β domain structure seen in the ADP-GK structures. A large conformational change accompanies binding of phosphoryl donor, acceptor, or both, in all members of the ribokinase superfamily characterized thus far, which is believed to be critical to enzyme function. Surprisingly, no such conformational change was observed in the AMP-bound *Ph*PFK structure compared with the apo structure. Through comprehensive site-directed mutagenesis of the substrate binding pocket we identified residues that were critical for both substrate recognition and the phosphotransfer reaction. The catalytic residues and many of the substrate binding residues are conserved between *Ph*PFK and ADP-GKs; however, four key residues differ in the sugar-binding pocket, which we have shown determine the sugar-binding specificity. Using these results we were able to engineer a mutant *Ph*PFK that mimics the ADP-GK/PFK and is able to phosphorylate both fructose 6-phosphate and glucose.

Glycolysis is a central and highly conserved metabolic pathway in all three domains of life. However, the Embden-Meyerhof glycolytic pathway of some hyperthermophilic archaea displays distinct differences from the classical pathway. Glyceraldehyde-3-phosphate is converted to 3-phospho (3P)-glycerate by glyceraldehyde-3-phosphate ferredoxin oxidoreductase in a single step instead of using glyceraldehyde-3-phosphate dehydrogenase and phosphoglycerate kinase in the classical two-step reaction mechanism (1, 2). Also, the classical ATP-dependent glucokinases (ATP-GKs)[3] and phosphofructokinases (ATP-PFKs) are replaced with novel ADP-dependent glucokinases and ADP-dependent phosphofructokinases or, in the case of *Methanococcus jannaschii*, a bifunctional ADP-dependent gluco-/phosphofructokinase (ADP-GK/PFK) (3–7).

PFKs convert fructose 6-phosphate (Fru-6-P) to fructose 1,6-bisphosphate. This is an early step in the Embden-Meyerhof pathway and therefore represents a critical control point for the entire pathway. Sequence and structural characterization classify PFKs into two convergent protein families (8): the PFK-A family and the ribokinase superfamily, which includes the PFK-B family and ADP-GK/ADP-PFK family. The PFK-A family includes both allosterically regulated ATP-dependent enzymes found in a variety of eukarya and bacteria and non-allosterically regulated PP_i-dependent enzymes found in all three domains of life (9, 10). The PFK-B family is a diverse family of ATP-dependent carbohydrate and pyrimidine kinases that is also present in all three domains of life. In general, ATP-PFKs from the PFK-B family can be differentiated from PFK-A ATP-PFKs by their lack of allosteric regulation, although the minor ATP-PFK from *Escherichia coli*, Pfk-2, is allosterically regulated by MgATP (12).

Several crystal structures of the PFK-A family PFKs have been reported. The best studied are the tetrameric PFKs from *E. coli* and *Bacillus stearothermophilus* (13, 14). Both contain subunits that consist of a large and a small 3-layered $\alpha\beta\alpha$ sandwich domain (13, 14). The large domain binds to ATP and the small domain binds to Fru-6-P (13, 14). Recently the crystal structure of Pfk-2, a member of the PFK-B family, was solved (15). It is composed of two domains, a large 3-layered $\alpha\beta\alpha$ sandwich

* This work was supported, in whole or in part, by National Institutes of Health Grant GM074942. This work was also supported by Genome Canada (through the Ontario Genomics Initiative), Fondo Nacional de Desarrollo Científico y Tecnológico (Fondecyt) Grant 1070111, the United States Department of Energy, Office of Biological Research, under contract DE-AC02-06CH11357, and the Canadian Institutes of Health Research.

[S] The on-line version of this article (available at http://www.jbc.org) contains supplemental data, Table S1, and Figs. S1 and S2.

The atomic coordinates and structure factors (codes 1U2X and 3DRW) have been deposited in the Protein Data Bank, Research Collaboratory for Structural Bioinformatics, Rutgers University, New Brunswick, NJ (http://www.rcsb.org/).

[1] These authors contributed equally to the results of this work.

[2] Canada Research Chair in Structural Biology. To whom correspondence should be addressed. Tel.: 613-533-6277; Fax: 613-533-2497; E-mail: jia@queensu.ca.

[3] The abbreviations used are: GK, glucokinase; PFK, phosphofructokinase; *Pf*, *Pyrococcus furiosus*; *Ph*, *Pyrococcus horikoshii*; *Tl*, *Thermococcus litoralis*; r.m.s., root mean square.

domain, similar to that seen in the PFK-A family protein structure mentioned above, and a smaller four-stranded β-sheet domain (15).

To date ADP-PFKs have been reported as non-regulated enzymes with Michaelis-Menten kinetics. This part of glycolysis is particularly interesting because with the presence of PFKs and fructose-1,6-bisphosphatase there is the possibility to produce futile cycling resulting in a net hydrolysis of nucleotide (ADP in the case of *thermococcales*) which, of course is undesirable because it would uncouple the metabolism. *E. coli* has overcome this problem by using a strong MgATP-induced inhibition when Fru-6-P is low in both of its PFKs: Pfk-1 from the PFK-A family and Pfk-2 from the ribokinase superfamily (16, 17). On the other hand, the archaea with the modified Embden-Meyerhof pathway seems to control this issue at the transcriptional level as, depending on the growth medium, either the production of PFK or fructose-1,6-bisphosphatase is turned off (18). In this way, regulation of PFK is not needed.

The crystal structures of the ADP-GK from *Pyrococcus horikoshii* (*Ph*GK), the ADP-GK from *Thermococcus litoralis* (*Tl*GK) bound to ADP, and the ADP-GK from *Pyrococcus furiosus* (*Pf*GK) in complex with AMP and glucose have been reported, although there are no crystal structures of ADP-PFK or the bifunctional ADP-GK/PFK (19–21). Despite low sequence identity between ADP-GKs and other kinases (*e.g.* *Ph*GK shares 11 and 12% identity with *E. coli* ribokinase and human adenosine kinase, respectively) the fold is similar to that of ribokinases (19). As a result, ADP-GKs have been classified as members of the ribokinase superfamily (19). Overall, ADP-GK structures are composed of a large and a small α/β domain (19–21). The ADP binding pocket is found on the surface of the large domain (19–21). Residues responsible for glucose binding are found on the surface of both the large and small domains adjacent to the ADP-binding pocket (19–21). Upon glucose binding, the protein undergoes a conformational change whereby the large and small domains close in creating the active-site pocket (20). Interestingly, the unique ADP binding pocket of ADP-GKs recognizes the α- and β-phosphate of the ADP in an almost identical manner to how the β- and γ-phosphate of ATP are recognized in ATP-dependent kinases of the ribokinase superfamily (19).

Here, we report the first structure of an ADP-PFK, alone and in complex with AMP, together with the biochemical characterization of the kinetic properties and substrate specificities. Moreover, we carried out site-directed mutagenesis in the sugar-binding pocket and active site of *Ph*PFK and identified residues that are critical for PFK activity and for distinguishing between glucose and Fru-6-P.

EXPERIMENTAL PROCEDURES

Cloning, Expression, and Protein Purification—The open reading frame for *Ph*PFK (PH1645) was amplified by PCR and inserted between the NdeI and BamHI restriction sites of a modified pET-15b expression vector (Novagen) (vector p11) as previously described (22). This construct generated an N-terminal hexahistidine tag joined to the *Ph*PFK protein by the TEV protease recognition site (ENLYFQ ↓ G). Recombinant wild type and mutant (see below) native and selenomethionine-labeled *Ph*PFK proteins were expressed in BL21(DE3) and DL41(DE3) *E. coli* cells (Novagen), respectively. Protein was purified using nickel-nitrilotriacetic acid affinity and size exclusion chromatographies. For more details see supplemental materials.

Site-directed Mutagenesis—Site-directed mutagenesis was performed using QuikChange™ site-directed mutagenesis kit (Stratagene) according to the manufacturer's protocol using the *Ph*PFK expression vector described above as the template. See Table 1 for the list of mutations made.

Protein Crystallization—Protein crystals of apo-*Ph*PFK were generated through hanging drop vapor diffusion at 21 °C by mixing 2 μl of protein solution (10 mg/ml) with 2 μl of well solution consisting of 22% PEG 4000, 0.1 M Tris-HCl, pH 8.5, and 0.2 M $LiSO_4$. Crystals of the *Ph*PFK complex with AMP were obtained by crystallization of the *Ph*PFK D17A protein in the presence of 20% PEG 3350, 0.2 M lithium citrate, 10 mM fructose 6-phosphate, and 5 mM ADP. Prior to data collection, crystals were transferred into Paratone-N and cryo-cooled in a nitrogen gas steam.

X-ray Diffraction, Structure Determination, and Refinement—Apo-*Ph*PFK crystals were placed in a cryoprotectant composed of 15% glycerol added to the crystallization solution and then flash frozen in liquid nitrogen prior to data collection. Multi-wavelength anomalous dispersion data were collected at three wavelengths 0.96396, 0.97918, and 0.97943 Å at the Advanced Photon Source (APS, Argonne, IL) beamline 19-ID of the Structural Biology Center-CAT with a SBC-3 CCD detector. The data were processed using HKL2000 (23). Data collection and processing statistics are shown in Table 2.

The structure of *Ph*PFK was solved using the multiwavelength anomalous dispersion method. Selenium sites were located using SOLVE (24, 25). Six of the 10 expected selenium sites per asymmetric unit were found. Selenium position refinement, phase calculation, and density modification was performed by SHARP (26). The structural model was built and refined by XFIT, CNS, and Refmac (27, 28). The AMP-bound structure was solved by molecular replacement using Phaser and the model was validated in Coot (29, 30). The final refinement statistics can be found in Table 2.

Determination of Enzyme Activity—PFK activity was assayed spectrophotometrically at 50 °C, by coupling the fructose-1,6-bisphosphate formation to the oxidation of NADH as previously described (3). See supplemental materials for more details.

Substrate Specificity—The phosphoryl group donor specificity of *Ph*PFK was determined by measuring the PFK activity as described above substituting ADP for the following phosphoryl group donors, UDP, IDP, GDP, and CDP. The activity is reported as percentage of the maximum activity obtained with ADP. The divalent cation preference was tested similarly, replacing $MgCl_2$ in the assay by $MgSO_4$, $MnCl_2$, $NiSO_4$, $CaCl_2$, or $ZnCl_2$. 2.5, 4, and 7 mM total metal were used, keeping other components as those used in the standard assay. The activity observed using these metals was reported as units/mg.

Kinetic Parameters—Kinetic parameters were determined at 50 °C by varying the concentrations of Fru-6-P (0 to 2 mM) with saturating ADP concentrations, and vice versa (3). For some

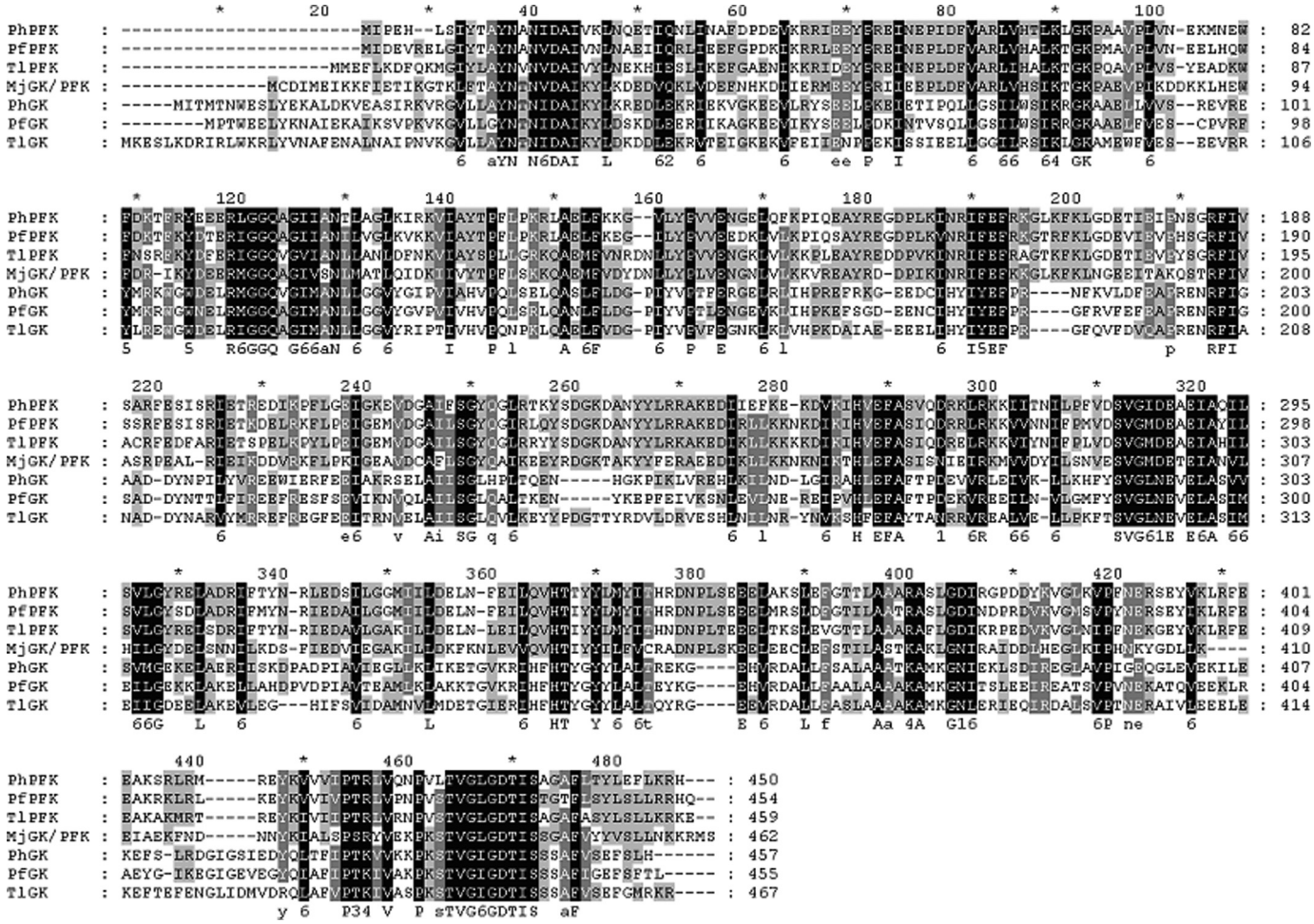

FIGURE 1. **Multiple sequence alignment of *Ph*PFK with other ADP-PFKs, ADP-GKs, and the bifunctional ADP-GK/PFK.** *Pf*, *P. furiosus*; *Ph*, *P. horikoshii*; *Tl*, *T. litoralis*; and *Mj*, *M. jannaschii*). This figure was prepared using GeneDoc (11).

mutants, the range of Fru-6-P concentrations was increased. In all these experiments, $MgCl_2$ was used as the divalent cation. The data were analyzed using SigmaPlot software (Systat Software, Inc., CA), and fitted to the Michaelis-Menten equation.

RESULTS AND DISCUSSION

Enzymatic Activity and Substrate Specificity of PhPFK—*Ph*PFK is predicted to be an ADP-PFK based on sequence similarity (Fig. 1). In addition, the *Ph*PFK structures align well with the available ADP-GK structures (Fig. 2, *C* and *D*). Therefore, to test whether this enzyme is a true ADP-PFK the phosphorylation of Fru-6-P was assayed in the presence of several nucleotides. PFK activity was the highest in the presence of ADP or UDP as the phosphoryl group donor (Fig. 3*A*). However, *Ph*PFK is also capable of transferring phosphoryl groups from IDP, GDP, and CDP to Fru-6-P but at a significantly slower rate (Fig. 3*A*). A saturation curve was generated for both ADP and UDP. The calculated k_{cat} K_m^{-1} value for UDP was 40 times higher than that of ADP, indicating a strong preference for ADP over UDP as the phosphoryl group donor.

Wild type *Ph*PFK displayed Michaelis-Menten kinetics at 50 °C. The following constants were determined using direct fit: K_m values of 15.2 ± 2.5 and 13.2 ± 2.4 μM for Fru-6-P and ADP, respectively, and a k_{cat} value of 45.5 ± 4.0 s^{-1}. All kinetic parameters are summarized in Table 1 and Fig. 3*B*. The temperature of these reactions is much lower than the optimal growth temperature of *P. horikoshii* and because temperature has a significant effect on enzyme kinetics, the constants calculated here may differ from the values at the optimal growth temperature. Unfortunately, the commercially available auxiliar enzymes for this reaction are from mesophilic sources hindering the use of high temperatures in the assay. On the other hand, due to the large amount of mutants characterized in this article the study would be prohibitively longer using a discontinuous assay to measure the kinetic parameters at higher temperatures. Nevertheless, most of the work published for other enzymes from this family uses the same strategy, making the data here directly comparable. The calculated K_m values for Fru-6-P and ADP for wild type *Ph*PFK are significantly lower than those of the ADP-PFK from *P. furiosus*, 2.3 and 0.11 mM, respectively (7). However, the K_m for Fru-6-P is similar to the K_m obtained for the bifunctional ADP-GK/PFK from *M. jannaschii*, 9.6 μM. But, the K_m for ADP is still much lower, 0.49 mM (6).

Divalent cations were required for *Ph*PFK activity. Five divalent metal cations were tested (magnesium was tested with two counter ions to discard any effect of the anion) using 2.5, 4, and 7 mM of total metal with 2 mM total ADP and 2 mM total Fru-6-P

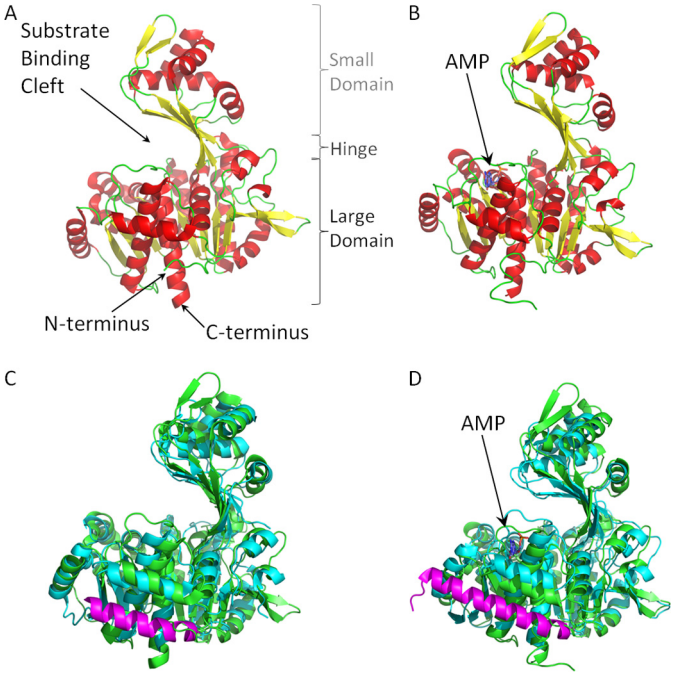

FIGURE 2. **Structure of apo- and AMP-bound *Ph*PFK and comparisons with ADP-GKs.** *A*, Apo-*Ph*PFK. *B*, AMP-bound *Ph*PFK. *C*, alignment of apo-*Ph*PFK structure (*green*) with *Ph*GK structure (*cyan*). The additional N-terminal α-helix of *Ph*GK not found in *Ph*PFK is shown in *magenta*. *D*, alignment of the AMP-bound *Ph*PFK structure (*green*) and the ADP-bound *Tl*GK structure (*cyan*). The additional N-terminal α-helix of *Tl*GK not found in *Ph*PFK is shown in *magenta*. This figure was generated using PyMOL.

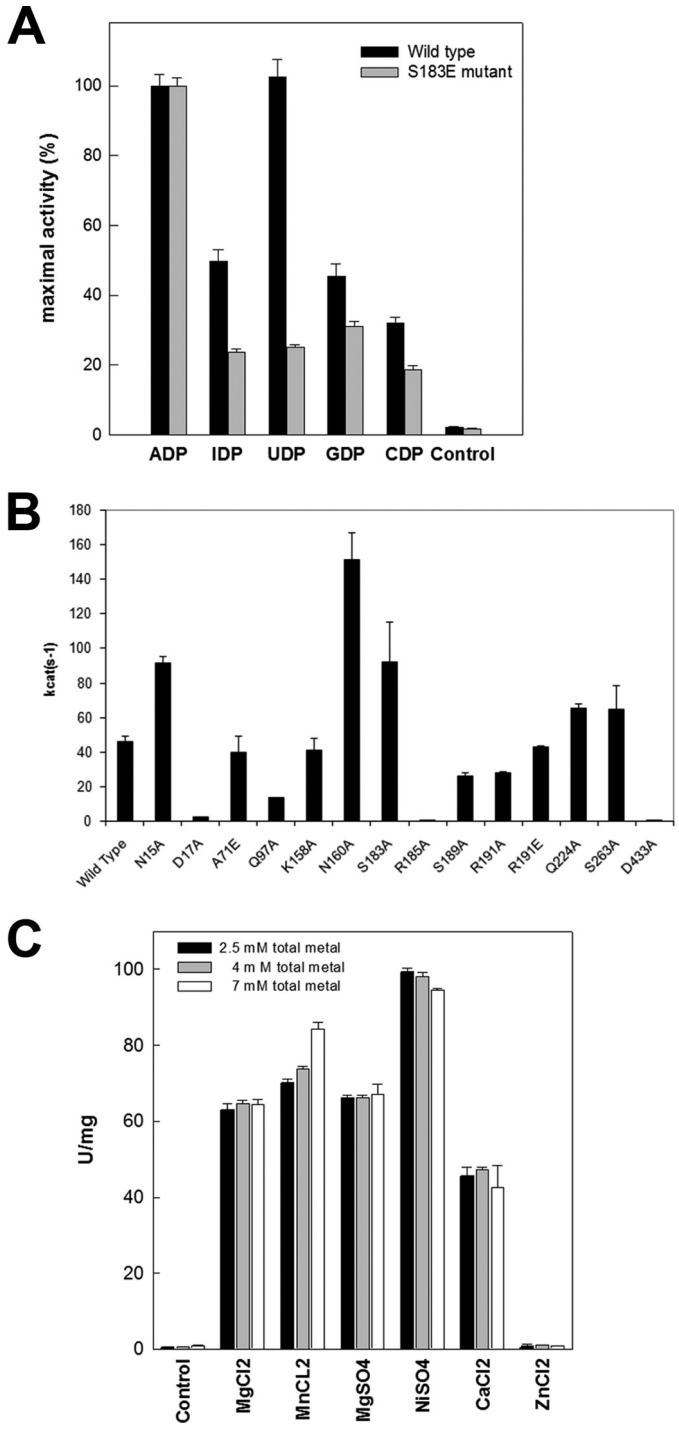

FIGURE 3. **PhPFK phosphoryl donor, kinetics, and divalent cation specificity.** *A*, wild type and S183E *Ph*PFK were assayed with different nucleotides as phosphoryl donors. The activity is shown as the percentage of the activity measured in the presence of ADP (100%). *B*, phosphofructokinase activity measurements were made for wild and mutant *Ph*PFKs. *C*, *Ph*PFK activity measured in presence of 2 mM Fru-6-P, 2 mM ADP, and the indicated divalent cation concentration. "*Control*" corresponds to the activity in the absence of nucleotide (*A*) and metal (*C*). Results are given as the mean ± S.E. of three experiments.

(Fig. 3*C*). In these conditions, the highest *Ph*PFK activity was obtained with $NiSO_4$ (~97 units/mg). The enzyme was also active in the presence of $MgCl_2$, $MnCl_2$, $MgSO_4$, and $CaCl_2$, but no significant activity was detected when the assay was performed in the presence of $ZnCl_2$. An increase in the enzyme activity, concomitantly with the increase in $MnCl_2$ concentration was observed, whereas the opposite effect was observed in the presence of $NiSO_4$. For the other divalent metals, the activity did not change with the cation concentration in the range tested. $CaCl_2$ showed the lowest activity with ~75% of the activity measured in the presence of $MgCl_2$. Although it is generally accepted that magnesium is the *in vivo* preferred metal, the ability of Ni^{2+}, Mn^{2+}, and to a lower extent Ca^{2+} to support *Ph*PFK activity with a high catalytic rate, suggests that other metals can substitute Mg^{2+}.

Overall Structure—The apo-*Ph*PFK structure (Fig. 2*A*) was refined to 2.0-Å resolution with $r = 0.177$ and $R_{free} = 0.226$ (Table 2). The structure contained 450 of the expected 474 residues from the expressed protein construct (Table 2). In the final model, 97.9% of the residues were in favored regions of the Ramachandran plot and none were in the disallowed region (Table 2). *Ph*PFK was crystallized alone and in complex with ADP. The apo structure was solved by the multiwavelength anomalous dispersion method using a selenomethionine derivative and the complex structure was solved by molecular replacement using the apo structure as a model. AMP, instead of ADP, was found in the active site. The AMP-bound structure (Fig. 2*B*) was refined to a resolution of 1.9 Å with $r = 0.177$ and $R_{free} = 0.228$ (Table 2). Both the apo- and AMP-bound *Ph*PFK crystal structures contained two molecules in the asymmetric unit. For a more detailed discussion of oligomeric state see supplemental materials.

The crystal structure of *Ph*PFK was aligned with *Ph*GK using the DaliLite server (Fig. 2*C*) (31). *Ph*PFK and *Ph*GK share 31%

TABLE 1
Kinetic parameters of wild type and mutant *Ph*PFKs

Enzyme	k_{cat}	K_m Fru-6-P	k_{cat}/K_m Fru-6-P	K_m ADP	k_{cat}/K_m ADP
	s^{-1}	μM	$M^{-1}\,s^{-1}$	μM	$M^{-1}\,s^{-1}$
Wild type	45.5 ± 4.0	15.2 ± 2.5	2.99×10^6	13.2 ± 2.4	3.45×10^6
N15A	91.1 ± 3.9	103 ± 1.4	8.84×10^5	23.8 ± 2.6	3.83×10^6
D17A	1.98 ± 0.0051	22600 ± 840	8.76×10^1	ND[a]	ND
A71E	39.3 ± 9.9	3.95 ± 0.2	1.72×10^6	13.6 ± 0.6	2.82×10^6
Q97A	13.0 ± 1.0	7.08 ± 0.74	1.84×10^6	7.47 ± 0.70	1.74×10^6
K158A	41.0 ± 6.7	6500 ± 1300	6.31×10^3	37.9 ± 6.7	1.08×10^6
N160A	151 ± 16	415 ± 13	3.64×10^5	72.4 ± 4.9	2.09×10^6
S183E	91.7 ± 23.6	86.5 ± 9	1.06×10^6	29.6 ± 2.2	3.10×10^6
R185A	0.351 ± 0.016	318 ± 9.5	1.10×10^3	473 ± 24	7.42×10^2
S189A	25.5 ± 2.6	9.02 ± 2.3	2.83×10^6	16.0 ± 1.2	1.60×10^6
R191A	27.4 ± 1.5	254.4 ± 26.1	1.07×10^5	14.5 ± 1.2	1.89×10^6
R191E	42.5 ± 1	4870 ± 173	8.73×10^3	60.5 ± 3.2	7.02×10^5
Q224A	65.3 ± 2.6	38.6 ± 1.3	1.69×10^6	29.5 ± 5.0	2.21×10^6
S263A	64.1 ± 14	39.5 ± 7.8	1.62×10^6	20.8 ± 3.4	3.08×10^6
D433A	0.00480 ± 0.00040	12.7 ± 4.2	3.78×10^2	13.9 ± 3.3	3.45×10^2

[a] ND, not determined. For the D17A mutant the kinetic parameters for MgADP were not determined because the elevated K_m value for Fru-6-P hinders reaching the saturating conditions.

TABLE 2
Crystallographic data and refinement statistics

$R_{sym} = \Sigma|I(k) - \langle I\rangle|/\Sigma I(k)$, where $I(k)$ and $\langle I\rangle$ represent the diffraction intensity values of the individual measurements and the corresponding mean values. The summation is over all measurements. Values in parentheses are for the highest resolution shell. PDB codes are 1U2X and 3DRW for apo-*Ph*PFK and its complex with AMP, respectively.

Structure	Apo-*Ph*PFK	Complex with AMP
Space group	$P2_1$	$P2_1$
Unit cell dimensions	a = 68.07, b = 99.93, c = 82.58 Å, β = 110.38°	a = 68.5, b = 104.2, c = 70.8 Å, β = 105.1°
Resolution range (Å)	40.0–2.0	41.5–1.9
Unique/free reflections (5%)	69,682/3,508	71,005/3,770
Completeness	99.2% (98.6%)	98.7% (90.7%)
R_{merge}	0.08 (0.445)	0.08 (0.353)
$I/\sigma(I)$	21.0 (3.57)	16.7 (3.25)
Redundancy	6.6 (5.9)	4.5 (3.9)
R_{cryst}/R_{free} (%)	20.2/24.5	17.3/22.1
R.m.s. deviation bond lengths (Å)	0.004	0.005
R.m.s. deviation bond angles (°)	0.609	0.705
Mean temperature factor (Å^2)	27.65	29.51

identity (Fig. 1). Overall, 407 residues were aligned, resulting in a *Z*-score and r.m.s. deviation between α-carbon positions of 39.9 and 2.5 Å, respectively. The AMP-bound *Ph*PFK structure was aligned with the ADP-bound *Tl*GK structure using the DaliLite server (Fig. 2*D*) (31). These two proteins also shared 31% identity with one another (Fig. 1). A total of 434 residues were aligned with a *Z*-score of 41.1 and a r.m.s. deviation between α-carbon positions of 3.3 Å. In both cases the structures were similar, sharing the same large and small α/β domain structures suggesting the common evolutionary origin of ADP-PFKs and ADP-GKs. However, the ADP-GK structures have an additional α-helix at their N termini and in the ADP-bound *Tl*GK structure, the small domain is closer to the large domain compared with AMP-bound *Ph*PFK. This is discussed further below.

Nucleotide and Mg^{2+} Binding Site—Overall, the apo- and AMP-bound *Ph*PFK structures show very little difference (r.m.s. deviation between α-carbon positions = 0.7 Å; *Z*-score = 61.9). However, AMP binding results in slight changes in the large nucleotide binding loop as well as the main chain positions of the β-sheet and loop that lie directly N-terminal to the large nucleotide binding loop (Fig. 4). A conformational change of

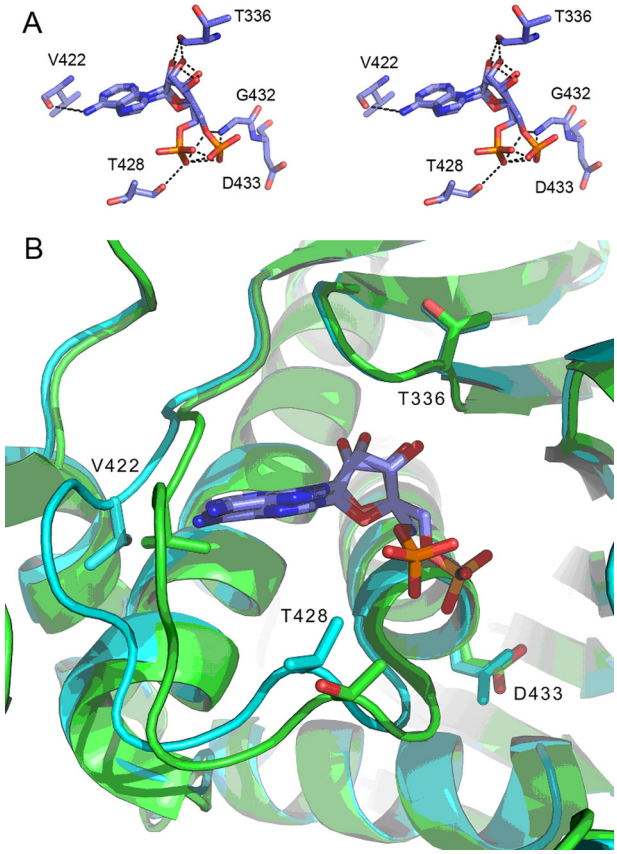

FIGURE 4. **AMP binding site of PhPFK.** *A*, stereo view of AMP-bound *Ph*PFK nucleotide binding site. *B*, comparison of the nucleotide binding site of apo- (*green*) and AMP-bound (*cyan*) *Ph*PFK. These figures were generated in PyMOL.

the large nucleotide binding loop was also reported upon ADP binding to *Tl*GK. There is good conservation between the nucleotide binding site of *Ph*PFK and ADP-GKs, however, some differences exist in the sugar-bound, closed conformation (threading model, see below). In the AMP- and glucose-bound *Pf*GK structure, Tyr-344 of the large domain hydrogen bonds with Glu-195 from the small domain. However, in *Ph*PFK the equivalent small domain residue, Ser-183, is too short to hydrogen bond with Tyr-338 of the large domain. This difference may account for the difference in phosphoryl group donor specific-

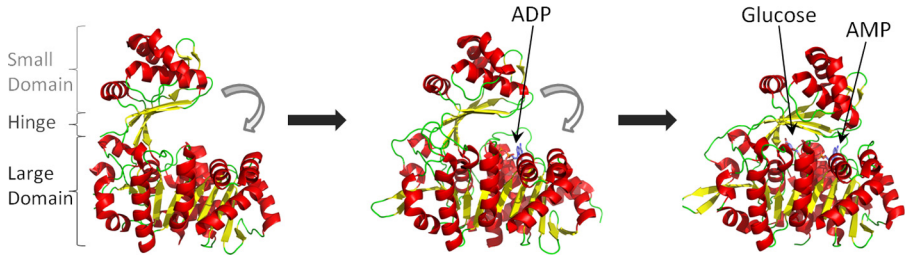

FIGURE 5. **Substrate-induced conformational changes of ADP-GKs.** *Left*, apo structure from *P. horikoshii* (21); *middle*, ADP-bound structure from *T. litoralis* (19); and *right*, AMP- and glucose-bound structure from *P. furiosus* (20).

ity in ADP-GKs and ADP-PFKs. ADP-PFKs are able to use GDP, to some extent, whereas ADP-GKs cannot. We made a S183E mutation and tested its ability to use different phosphoryl donors compared with the wild type enzyme (Fig. 3*A*). There was no difference in activity between the mutant and wild type using ADP as a phosphoryl donor. However, the S183E mutant displayed significantly less activity when the phosphoryl donor was replaced with IDP, UDP, GDP, or CDP, compared with the wild type.

One of the most intriguing features of these enzymes is the position in that they can bind ADP in a way that both α- and β-phosphates are recognized mainly in the same way as the β- and γ-phosphates in the ATP-dependent enzymes. In this respect, it has been proposed that the presence of a bulky side chain in the bottom of the nucleotide binding crevice (Tyr-357 in the case of *T. litoralis* ADP-GK), below the sugar part of the molecule, could account for the change in specificity (20). Moreover, it was proposed that because ADP-PFKs have leucine or isoleucine in this position they can marginally use ATP as phosphoryl donor as it was seen for the enzyme from *P. furiosus* (7). Because the corresponding lateral chain of *Ph*PFK (Leu-340) is placed in the corresponding position we tested directly the ability of this enzyme to use ATP using the pyruvate kinase/lactate dehydrogenase-coupled assay, which specifically consumes the ADP produced. Surprisingly, no activity was detected with this nucleotide.

Almost all phosphate transferring enzymes have Mg^{2+} in their active site thereby assisting with the phosphate transfer through interactions with the β- and γ-phosphate groups of ATP or the β-phosphate of ADP, when ADP is the phosphoryl group donor. However, Mg^{2+} was not observed in the *Ph*PFK structure or any of the ADP-GK structures. Although, 17 water molecules were trapped in the AMP- and glucose-bound *Pf*GK structure, which offers sufficient space for both a magnesium ion and the β-phosphate of ADP. Despite the prerequisite for Mg^{2+}, this cation has never been observed in the structure of a member of this superfamily, including *Ph*PFK.

Reaction Mechanism—A conserved aspartate residue in ribokinases, adenosine kinases, ADP-GKs, ADP-PFKs, and ADP-GK/PFK is believed to be the catalytic base involved in the phosphotransfer reaction of these kinases (Fig. 1). Mutations of this residue in *Tl*GK resulted in a significant reduction of glucokinase activity (20). Similarly, mutation of the corresponding aspartate in *Ph*PFK (Asp-433) to alanine resulted in a loss of PFK activity (Table 1).

Furthermore, a conserved arginine residue that approaches the active site during the domain closing event associated with sugar binding is believed to attract the terminal phosphate group of the phosphoryl donor, stimulating cleavage of the phosphodiester bond and transfer of the phosphate group. Mutation of Arg-205 in *Tl*GK to alanine resulted in <0.1% the activity of the wild type enzyme (20). We observed the same effect upon mutation of the corresponding arginine residue in *Ph*PFK (Arg-185) to alanine (Table 1). These two findings support a conserved mechanism among ADP-GKs, ADP-PFKs, and ADP-GK/PFKs.

Substrate-induced Fit—A large conformational change occurs in ADP-GKs as well as ATP-dependent hexokinases/glucokinases and ribokinases upon binding their respective substrates (Fig. 5) (20, 32–35). The flexible loops located between the large and small domains form a hinge that folds, closing the cleft between the two domains upon substrate binding (20, 32–35). This conformational change appears to be essential for positioning the catalytic residues of ADP-GKs and ribokinases (20, 34). The three ADP-GKs structures all display varying amounts of domain closure (Fig. 5) (19–21). The apo-*Ph*GK is the most open conformation (Fig. 5) (21). There is a rotation of about 20° between the large and small domain in the ADP-bound *Tl*GK structure compared with the *Ph*GK structure and an additional 20° rotation between the two domains in the AMP- and glucose-bound *Pf*GK structure compared with the *Tl*GK structure (Fig. 5) (19–21). It was initially reported that the *Tl*GK structure was the most open conformation because they were able to successfully soak ADP out of the crystal, which indicates the absence of a large conformational change (19). The *Ph*GK structure clearly presented a more open conformation, which led to the suggestion that *Tl*GK had been trapped in the ADP-bound conformation following the removal of the ADP from the crystal (21). However, ADP could not be soaked into the *Ph*GK crystal, which is thought to be due to an ADP-dependent domain closing (21). Interestingly, no such conformational change was observed between the apo- and AMP-bound *Ph*PFK structures. It could be that the β-phosphate of ADP is required to fully induce this conformational change. The amine nitrogen of Arg-205 from *Tl*GK is 3.8 Å away from the β-phosphate of ADP and may form important interactions that help to stabilize a more closed conformation (19). One other possibility is that for *Ph*PFK both co-factor and substrate are required for the conformational change observed as seen in other structures. In any case, the lack of conformational change in *Ph*PFK in the presence of AMP is somewhat surprising given the structure is from co-crystallization instead of soaking.

Sugar-binding Site—Attempts to co-crystallize or soak crystals with Fru-6-P or fructose-1,6-bisphosphate both in the presence or absence of ADP or nonhydrolyzable ADP analogues were unsuccessful. Due to the overall similarity between the *Ph*PFK structures and ADP-GKs structures, we modeled

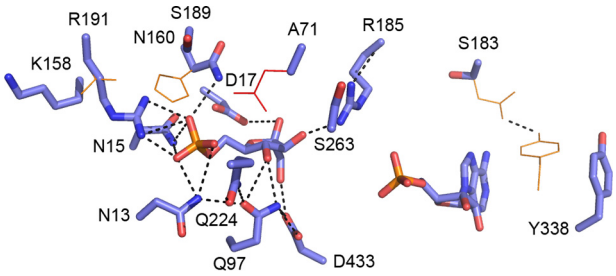

FIGURE 6. **Model of *Ph*PFK bound to Fru-6-P and AMP.** Docking model of the *Ph*PFK·Fru-6-P complex. Where different, the positions of residues conserved in ADP-GKs are shown in *orange*. The *red* residue corresponds to the glutamate residue conserved in the bifunctional ADP-GK/PFK (Glu-82) and in ADP-GKs (Glu-88). *Black dotted lines* represent hydrogen bonding.

*Ph*PFK in the closed conformation bound to Fru-6-P and AMP based on the AMP- and glucose-bound *Pf*GK structure (Fig. 6). The primary sequence of *Ph*PFK was threaded onto the *Pf*GK structure bound to both AMP and glucose, and the resulting model was energy minimized. Fru-6-P was docked with the structure using AutoDock (36). All of the 10 lowest energy docking results placed the phosphate in the same position with only slight differences in the placement of the sugar moiety.

To validate our model and gain further insights into substrate specificity, relevant residues from the Fru-6-P binding pocket of *Ph*PFK, the highly conserved residues Asn-15, Asp-17, Gln-97, Lys-158, Asn-160, Arg-185, Ser-189, Arg-191, Gln-224, Ser-263, and Asp-443 were mutated to alanine to establish their importance to substrate binding and catalysis. Of these, N15A, D17A, K158A, N160A, R185A, and R191A show the most significant increase in their K_m value for Fru-6-P (Table 1). Asn-160, Asn-15, and Arg-191 form one, two, and three hydrogen bonds with the phosphate group of Fru-6-P, respectively, as judged by the docked conformation (Fig. 6). Arg-185 and Asp-17 form hydrogen bonds with the sugar moiety of Fru-6-P (Fig. 6). As a result, loss of these interactions weakens *Ph*PFK binding to its substrate. Lys-158 is too far to hydrogen bond with the phosphate of Fru-6-P in our model (Fig. 6). However, it is strictly conserved in PFKs and mutation of this residue has the most significant effect on Fru-6-P binding after the D17A mutation (Table 1). There are several possible explanations for this observation; however, it is most likely a result of the threading procedure itself, because there is no negative charge to stabilize the positive lateral chain of Lys-158 inside the binding pocket and therefore repelling it in the opposite direction. In fact, simple rotation of the side chain of Lys-158 in our model would result in a distance of less than 3.5 Å to the phosphate group of Fru-6-P. This was confirmed using a molecular dynamics simulation (see supplemental materials). In this conformation, the lateral chains of Lys-158 and Arg-191 could form a salt bridge with the phosphate group of Fru-6-P, which would explain the behavior of the mutant enzyme.

Interestingly, the half of the sugar ring opposite to the endocyclic oxygen is recognized mainly in the same way as the comparable part of glucose by ADP-GKs. As expected the residues responsible of this like Asn-15, Asp-17, and Gly-96 are conserved in both specificities. As can be seen below, the sugar discrimination comes mainly by the interactions with the other half of the ring. This suggests that the sugar-binding site in the family is strongly plastic to accommodate a furanose-P and a pyranose with mainly the same residues, but still very selective to precisely discriminate between the two of them. Q224A and S263A contribute little to the sugar binding: both mutations result in small increases in K_m for Fru-6-P of about 2–3-fold (Table 1). Surprisingly, Q97A, S189A, and D433A mutations lead to a small decrease in K_m for Fru-6-P despite the loss of a hydrogen bond in the case of Q97A and D433A (Table 1). Also, Arg-185 and Asp-433 make contact with the C1 hydroxyl group, which supports the proposed catalytic mechanism. However, due to the lack of the phosphate group from ADP, the position of Arg-185 could be somewhat distorted. Nevertheless, our model is well supported by the mutational data.

Differences between ADP-PFKs and ADP-GKs—The conserved residues Asn-13, Asn-15, Asp-17, Gly-96, Gln-97 and Arg-185 form hydrogen bonds with Fru-6-P, as shown in Fig. 6*A*. Lys-158, Asn-160, and Arg-191 also form hydrogen bonds with Fru-6-P (Fig. 6). These residues are present in the bifunctional ADP-GK/PFK from *M. jannaschii* but the equivalent residues in ADP-GKs are non-conserved small residues, histidine and aspartate, respectively. A similar scenario was seen in a previous *in silico* study using the bifunctional enzyme from *M. jannaschii* (37). The positive charge on Arg-191 of *Ph*PFK attracts the phosphate group of Fru-6-P, and is still compatible with glucose binding. However, when replaced by aspartate in ADP-GKs, the negatively charged side chain likely repels the phosphate group of Fru-6-P, which prevents ADP-GKs from binding Fru-6-P. To assess the role of Arg-191 in Fru-6-P binding, we made two mutations, R191A and R191E. The R191A mutation removes three hydrogen bonds to the phosphate group on Fru-6-P and causes a ~17-fold increase in the K_m value for Fru-6-P (Table 1). However, as predicted, the charge reversal of the R191E mutation has a much more pronounced effect on Fru-6-P binding, a ~325-fold increase in K_m (Table 1). Even so, the R191E mutant enzyme is not able to phosphorylate glucose, suggesting that the presence of this charged residue in the bottom of the sugar-binding site in all ADP-GKs contribute to sugar discrimination by hindering the protein from binding Fru-6-P and not by increasing the affinity for glucose.

The key difference between kinases that are capable of phosphorylating glucose and those that cannot is a conserved glutamate residue found in ADP-GKs (Glu-88 from *Pf*GK) and ADP-GK/PFK (Glu-82) that is replaced with alanine in *Ph*PFK (Ala-71). In the *Pf*GK-glucose-AMP complex structure, the Glu-88 lateral chain forms a hydrogen bond with the C2 hydroxyl group of the bound glucose molecule. This interaction is thought to be critical for orienting the glucose molecule in the active site and it has also been highlighted as crucial for the sugar specificity in the past (6, 13, 37). As a result, ADP-PFKs cannot phosphorylate glucose. We tested this hypothesis by mutating Ala-71 to glutamate. As expected, this mutation has little effect on Fru-6-P binding compared with the wild type (Table 1). However, the A71E mutant enzyme can also bind glucose (K_m = 3.95 ± 0.2 mM) and is capable of phosphorylating glucose (k_{cat} of 2.68 ± 0.05 s^{-1}) (Table 1). In contrast, the wild type enzyme displays no activity for glucose. This result demonstrates that Ala-71 is a key player in determining substrate specificity. Interestingly, the catalytic mechanism

described before for the *Ph*PFK seems to be even more general because comparison of these features with the non-homologous ATP-dependent PFK (Pfk-1) from *E. coli* pointed out striking similarities.

In terms of catalysis, in Pfk-1, Asp-127 plays a critical role as a general base, increasing the nucleophilicity of the 1-hydroxyl of Fru-6-P by abstracting its proton and permitting attack on the γ-phosphate of the substrate ATP in a similar way as Asp-433 in *Ph*PFK (38). In addition, Arg-162 and Arg-243 interact with the 6-phosphate of Fru-6-P. Truncation of these residues to serine results in enzymes with decreased Fru-6-P binding ability and reduced cooperativity, but little change in catalytic ability in a very similar way to Lys-158 and Arg-191 (39). Then, it would appear that some structural features related to catalysis in ADP-dependent PFK have analogous counterparts in the ATP PFKs.

Conclusion—In summary, we determined the first crystal structure of an ADP-dependent phosphofructokinase both alone and in complex with AMP and through comprehensive mutagenesis we identified residues that were critical for both the phosphotransfer reaction and substrate binding. Our results demonstrate that the overall structure of ADP-PFK is similar to that of ADP-GK and that the two share a common mechanism of action. However, unlike the available ADP-GK structures, no conformational change was observed upon nucleotide binding. This was unexpected and may indicate that the nucleotide-dependent conformational change is a non-essential part of the ADP-dependent sugar kinase mechanism. Moreover, we identified four key residues responsible for the sugar binding specificity. Using this knowledge, we were able to generate a mutant *Ph*PFK that is capable of phosphorylating both Fru-6-P and glucose.

Acknowledgments—We thank all members of the Ontario Centre for Structural Proteomics (Structural Proteomics in Toronto, SPiT) for help in conducting experiments. We also thank Dr. Richard C. Garratt from the Instituto de Física de São Carlos, Universidade de São Paulo, Brasil, where the Dynamic Light Scattering experiments were performed.

REFERENCES

1. Mukund, S., and Adams, M. W. W. (1995) *J. Biol. Chem.* **270,** 8389–8392
2. van der Oost, J., Schut, G., Kengen, S. W., Hagen, W. R., Thomm, M., and de Vos, W. M. (1998) *J. Biol. Chem.* **273,** 28149–28154
3. Kengen, S. W., de Bok, F. A., van Loo, N. D., Dijkema, C., Stams, A. J., and de Vos, W. M. (1994) *J. Biol. Chem.* **269,** 17537–17541
4. Kengen, S. W., Tuininga, J. E., de Bok, F. A., Stams, A. J., and de Vos, W. M. (1995) *J. Biol. Chem.* **270,** 30453–30457
5. Koga, S., Yoshioka, I., Sakuraba, H., Takahashi, M., Sakasegawa, S., Shimizu, S., and Ohshima, T. (2000) *J. Biochem.* **128,** 1079–1085
6. Sakuraba, H., Yoshioka, I., Koga, S., Takahashi, M., Kitahama, Y., Satomura, T., Kawakami, R., and Ohshima, T. (2002) *J. Biol. Chem.* **277,** 12495–12498
7. Tuininga, J. E., Verhees, C. H., van der Oost, J., Kengen, S. W., Stams, A. J., and de Vos, W. M. (1999) *J. Biol. Chem.* **274,** 21023–21028
8. Bateman, A., Birney, E., Durbin, R., Eddy, S. R., Howe, K. L., and Sonnhammer, E. L. L. (2000) *Nucleic Acids Res.* **28,** 263–266
9. Hansen, T., Musfeldt, M., and Schönheit, P. (2002) *Arch. Microbiol.* **177,** 401–409
10. Meyer, C., Schmid, R., Scriba, P. C., and Wehling, M. (1996) *Eur. J. Biochem.* **239,** 726–731
11. Nicholas, K. B., Nicholas, H. B., Jr., and Deerfield, D. W., II (1997) *GeneDoc: Analysis and Visualization of Genetic Variations, EMBNEW. NEWS* **4,** 14
12. Guixé, V., Rodríguez, P. H., and Babul, J. (1998) *Biochemistry* **37,** 13269–13275
13. Evans, P. R., Farrants, G. W., and Hudson, P. J. (1981) *Philos. Trans. R. Soc. Lond. B Biol. Sci.* **293,** 53–62
14. Schirmer, T., and Evans, P. R. (1990) *Nature* **343,** 140–145
15. Cabrera, R., Ambrosio, A. L., Garratt, R. C., Guixé, V., and Babul, J. (2008) *J. Mol. Biol.* **383,** 588–602
16. Torres, J. C., Guixé, V., and Babul, J. (1997) *Biochem. J.* **327,** 675–684
17. Zheng, R. L., and Kemp, R. G. (1992) *J. Biol. Chem.* **267,** 23640–23645
18. Schut, G. J., Brehm, S. D., Datta, S., and Adams, M. W. W. (2003) *J. Bacteriol.* **185,** 3935–3947
19. Ito, S., Fushinobu, S., Yoshioka, I., Koga, S., Matsuzawa, H., and Wakagi, T. (2001) *Structure* **9,** 205–214
20. Ito, S., Fushinobu, S., Jeong, J. J., Yoshioka, I., Koga, S., Shoun, H., and Wakagi, T. (2003) *J. Mol. Biol.* **331,** 871–883
21. Tsuge, H., Sakuraba, H., Kobe, T., Kujime, A., Katunuma, N., and Ohshima, T. (2002) *Protein Sci.* **11,** 2456–2463
22. Zhang, R. G., Skarina, T., Katz, J. E., Beasley, S., Khachatryan, A., Vyas, S., Arrowsmith, C. H., Clarke, S., Edwards, A., Joachimiak, A., and Savchenko, A. (2001) *Structure* **9,** 1095–1106
23. Otwinowski, Z., and Minor, W. (1997) *Methods Enzymol.* **276,** 307–326
24. Terwilliger, T. C. (2000) *Acta Crystallogr. D Biol. Crystallogr.* **56,** 965–972
25. Terwilliger, T. C., and Berendzen, J. (1999) *Acta Crystallogr. D Biol. Crystallogr.* **55,** 849–861
26. Fortelle, E. D. L., and Bricogne, G. (1997) *Methods Enzymol.* **276,** 472–493
27. Brünger, A. T., Adams, P. D., Clore, G. M., DeLano, W. L., Gros, P., Grosse-Kunstleve, R. W., Jiang, J. S., Kuszewski, J., Nilges, M., Pannu, N. S., Read, R. J., Rice, L. M., Simonson, T., and Warren, G. L. (1998) *Acta Crystallogr. D Biol. Crystallogr.* **54,** 905–921
28. McRee, D. E. (1999) *J. Struct. Biol.* **125,** 156–165
29. Emsley, P., and Cowtan, K. (2004) *Acta Crystallogr. D* **60,** 2126–2132
30. McCoy, A. J., Grosse-Kunstleve, R. W., Adams, P. D., Winn, M. D., Storoni, L. C., and Read, R. J. (2007) *J. Appl. Crystallogr.* **40,** 658–674
31. Holm, L., and Park, J. (2000) *Bioinformatics* **16,** 566–567
32. Anderson, C. M., Stenkamp, R. E., and Steitz, T. A. (1978) *J. Mol. Biol.* **123,** 15–33
33. Mulichak, A. M., Wilson, J. E., Padmanabhan, K., and Garavito, R. M. (1998) *Nat. Struct. Biol.* **5,** 555–560
34. Sigrell, J. A., Cameron, A. D., Jones, T. A., and Mowbray, S. L. (1998) *Structure* **6,** 183–193
35. St. Charles, R., Harrison, R. W., Bell, G. I., Pilkis, S. J., and Weber, I. T. (1994) *Diabetes* **43,** 784–791
36. Morris, G. M., Goodsell, D. S., Halliday, R. S., Huey, R., Hart, W. E., Belew, R. K., and Olson, A. J. (1998) *J. Comput. Chem.* **19,** 1639–1662
37. Merino, F., and Guixé, V. (2008) *FEBS J.* **275,** 4033–4044
38. Hellinga, H. W., and Evans, P. R. (1987) *Nature* **327,** 437–439
39. Berger, S. A., and Evans, P. R. (1990) *Nature* **343,** 575–576